JOURNAL OF CHEMICAL ENGINEERING AND INDUSTRIAL BIOTECHNOLOGY
e-ISSN: 0126-8139
Volume 12, Issue 1, 2026, 7 - 17
DOI: https://doi.org/10.15282/jceib.v12i1.13302

RESEARCH ARTICLE

# Hydrodynamic characterisation in a flat-panel photobioreactor through computational fluid dynamics analysis

**Nur Aqila Syafiqa Abdul Nuri[1], Noor Illi Mohamad Puad[1]*, Azlin Suhaida Azmi[1], Farah Ahmad[1], Hasrizal Abd Rahman[2], Ahmad Afiq Arshad Nasharuddin[3]**

[1]Department of Chemical Engineering and Sustainability, Kulliyyah of Engineering, International Islamic University Malaysia, 50728 Kuala Lumpur, Malaysia
[2]PETRONAS Research Sdn. Bhd., Lot 3288 & 3289, Off Jalan Ayer Itam, Kawasan Institusi Bangi, 43000 Kajang, Selangor, Malaysia
[3]Faculty of Chemical and Energy Engineering, Universiti Teknologi Malaysia, 81310 Skudai, Johor, Malaysia

**Abstract -** Assessing hydrodynamic parameters in photobioreactors (PBR) is essential for optimised operation, yet computational fluid dynamics studies specifically evaluating shear stress properties remain scarce. This study utilises COMSOL Multiphysics® to provide novel quantitative insights into the hydrodynamic performance of a 15 L conventional flat-panel photobioreactor. A 2D time-dependent turbulent bubbly-flow model based on the Euler-Euler approach was implemented and validated against an airlift PBR (ALR) system, with a margin of error of less than 3%. Fluid flow, shear stress, and mixing behaviour were systematically investigated under aeration rates ranging from 0.1 to 1.0 vvm. Results demonstrated that while increasing aeration improved hydrodynamic parameters, average liquid velocities consistently remained below 0.02 m/s, indicating the persistent presence of dead zones near the vessel walls. Crucially, simulated shear stress remained below the 1.2 Pa critical threshold for microalgal cell damage. However, the 0.2 Pa threshold required to inhibit biofilm formation was only exceeded at aeration levels above 0.4 vvm. While higher aeration increased average turbulent kinetic energy and turbulent energy dissipation, their distribution remained non-uniform, with peak turbulence concentrated near the sparger and upper sections. These findings suggest an optimal aeration range of 0.2 to 0.6 vvm to balance mixing efficiency and shear control. Ultimately, this work delivers novel quantitative mapping of critical hydrodynamic regions, advancing the predictive basis for reactor scale-up and design optimisation.

**Article History**
Received : 5 November 2025
Revised : 31 March 2026
Accepted : 2 April 2026
Published : 30 April 2026

**Keywords**
*Photobioreactor*
*Computational fluid dynamics*
*Hydrodynamics*
*COMSOL Multiphyiscs®*

## 1. Introduction

Microalgal cultivation in a photobioreactor (PBR) system plays a significant role in combating carbon emissions. The cultivation process, via diverse pathways including autotrophic, heterotrophic, and mixotrophic modes, is primarily carried out by utilising carbon dioxide ($CO_2$) and light to support microalgal growth [1]-[2]. The key advantage of microalgae cultivation over other carbon capture techniques is the production of value-added biomass. This value-added product is valuable as it can be used for other applications, such as animal feed and pharmaceutical products. This is because the biomass produced contains a significant amount of proteins, carbohydrates, and lipids [3]-[4]. PBR systems can be categorised into two distinct groups: open and closed systems. The closed system PBRs were developed to address the drawbacks of open systems, such as uncontrollable operating conditions and greater susceptibility to contamination. These drawbacks are vital because they contribute to poor $CO_2$ fixation efficiency and low biomass productivity [5]-[6]. One prevalent type of closed-system PBR is the flat-panel or flat-plate PBR (FPPBR). FPPBR has been utilised to grow a variety of microalgae at different scales for various applications due to its distinctive features, including a short light path and a simple design [7]-[8]. Nevertheless, many parameters are involved in PBR operation, including physicochemical and hydrodynamic parameters, which limit the broader application of closed-system PBR at larger scales. Hence, depending solely on experimental analysis for further investigation is time-consuming and expensive. As a result, numerous researchers have utilised computational fluid dynamics (CFD) analysis to better understand PBR operation [9]–[11]. This numerical analysis is an effective approach to assessing the hydrodynamic performance of PBR systems by examining multiple fluid-flow variables, including fluid velocity, turbulent kinetic energy (TKE), and the mass transfer coefficient. This has reduced the number of experiments required and produced more reliable systems [9, 12]. Generally, past studies on CFD simulation in PBR systems have primarily utilised ANSYS software to evaluate hydrodynamic conditions [10]-[11]. Exploring different software can be useful for gaining additional perspectives, as they may use distinct discretisation techniques. For instance, ANSYS is a finite-volume application, while COMSOL is a finite-element application. Table 1 summarises the available literature that has used COMSOL software to conduct CFD simulations in PBR systems, which remains scarce. A few successful CFD applications in COMSOL for the design of PBRs have been reported, serving different purposes, including structural optimisation and light integration. Moreover, complex simulations integrating fluid dynamics with other submodels have been observed [13]-[14]. Nonetheless, based on the reviewed literature, there is potential for future development of CFD for PBR design, particularly for visualising the PBR system's flow field, and additional parameters should be investigated.

Additionally, based on the available knowledge, there are still limited studies on shear stress properties in FPPBR

***CORRESPONDING AUTHOR | N.I.M. Puad** | ✉ illi@iium.edu.my

using CFD analysis. Anyhow, shear stress is a significant limitation in FPPBR operation due to aeration, as highlighted in previous studies [7], [15]-[16]. Monitoring and controlling shear stress in PBR is crucial to ensure stable, optimised operation for microalgae to grow. Therefore, based on the identified research gaps, the present study aims to provide further fundamental insights into the hydrodynamic properties of a conventional FPPBR using COMSOL software. Specifically, key hydrodynamic characteristics, including fluid flow, shear stress, and mixing behaviour within the FPPBR, will be systematically investigated. This work further provides novel quantitative insights into shear stress distribution and turbulence behaviour that have not been systematically reported in previous studies.

Table 1. Recent literature on CFD studies

| Type of PBR | Controlled parameter | Observed parameter | Reference |
|---|---|---|---|
| 2-panel FPPBR | Geometric configurations and operating parameters | Flow field and microalgae concentration | [17] |
| Tubular PBR | Wall turbulence promoter | Velocity field, average power spectrum (representing mixing conditions), pressure drop, and energy consumption | [18] |
| Tubular PBR | Mixing method | Velocity field, pressure drop, swirl number, and frequencies of particle movement | [19] |
| Traditional FPPBR | Recycling gas flow rate and sparger design | Friction velocity, dead zone, power input, bubble volume fraction, biomass concentration, and bisabolene production | [13] |
| FPPBR | Design of FPPBR | Velocity field | [20] |
| Raceway reactor | Geometric configurations | Velocity profile, residence time, dead zone, and Cell Reynolds Number | [21] |
| Traditional FPPBR | Light source positioning | Light transmission | [14] |

## 2. Materials and Methods

### 2.1 Description of Flat Panel Photobioreactor

In this study, CFD was used to investigate the performance of a conventional FPPBR, with a primary focus on fluid velocity and shear stress. This evaluation was conducted at different aeration rates (0.1 to 1.0 vvm), defined based on variations in inlet gas velocity (Table 2). This range was selected because it is a considerable value of aeration rate for optimal operation of FPPBR, considering flow, shear stress, and mass transfer properties [22]–[25]. Several studies have emphasised the importance of aeration rate across diverse PBR operations, leading to its selection as the manipulated variable for this study. Before evaluating the FPPBR, validation procedures were conducted for the airlift PBR (ALR) system to ensure the reliability of the model to be implemented. This system was selected because there is insufficient detailed experimental data available, and only data from Sadeghizadeh et al. [26] this source are suitable for direct validation in this study. The study describes the effect of variation in gas superficial velocity on hydrodynamic parameters and $CO_2$ fixation by microalgae grown in the ALR system.

Table 2. Variation of inlet gas velocity for the analysis of FPPBR performance

| Air flow rate, vvm | Inlet gas velocity, $V_i$ (m/s) |
|---|---|
| 0.1 | 0.0005 |
| 0.2 | 0.001 |
| 0.4 | 0.002 |
| 0.6 | 0.003 |
| 0.8 | 0.004 |
| 1.0 | 0.005 |

### 2.2 Description of Geometry

Figure 1(a) shows the overall schematic diagram of the system investigated in this study. The system of interest is a 15 L conventional FPPBR with a cuboidal shape, measuring 250 mm (length) x 150 mm (width) x 400 mm (height). The vessel is equipped with a bottom sparger as a gassing unit, consisting of 20 evenly distributed 0.5-mm holes. Furthermore, an ALR system with a 20 L working volume was employed for the validation case (Figure 1(b)). The structures of both systems are similar, except that the ALR system is internally divided into riser and downcomer sections to direct fluid flow within the vessel for better mixing.

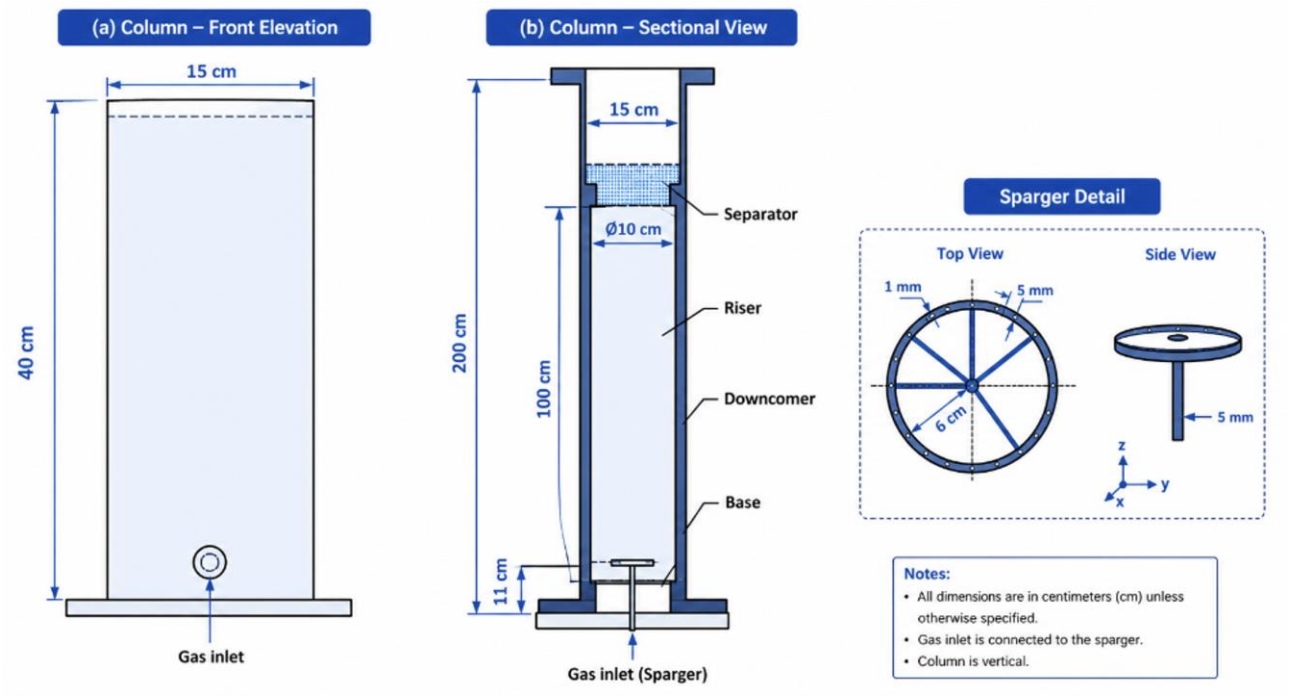


Figure 1. Geometrical representation of: (a) conventional FPPBR adopted from Huang et al. [27], copyright 2014, with permission from Elsevier (5692691427530), and (b) ALR adapted from Sadeghizadeh et al. [26], copyright 2017, with permission from Elsevier (5692700081749)

### 2.3 Governing Equations

This study used a *k*-*ε* turbulent bubbly-flow interface for CFD analysis. The bubbly flow model is based on the Euler-Euler approach, which relies on the following assumptions [20, 28]. The liquid and gas phases may be considered as interpenetrating media, with each phase having a distinct velocity field. Gas density is negligible compared to liquid density. A balance between viscous drag and pressure forces determines the motion of the gas bubble relative to the liquid. The two phases share the same pressure field. Assumptions are applied to the Euler-Euler model to simplify the equations that govern the mechanisms involved. Drawing from these presumptions, the momentum and continuity equations for both phases may be combined, while a gas-phase transport equation remains to oversee the volume proportion of bubbles. The detailed governing equations for the turbulent bubbly flow model of the liquid and gas phases are summarised in Table 3 (Eqs. 1-10).

Table 3. Governing equations for two-phase flow (bubbly flow turbulence model) for Newtonian fluid, isothermal, incompressible, and unsteady-state flow (Adapted from COMSOL Inc. Version 6 (2021)[29])

| Flow model | Equations | |
|---|---|---|
| Momentum equation | $\emptyset_l \mathrm{p_l} \frac{\partial \boldsymbol{u_l}}{\partial t} + \emptyset_1 \mathrm{p_l} \boldsymbol{u_l} . \nabla \boldsymbol{u_l} = -\nabla p + \nabla . \left[ \emptyset_l (\mu_l + \mu_T) \left( \nabla \boldsymbol{u_l} + \nabla \boldsymbol{u_l}^T - \frac{2}{3} (\nabla . \boldsymbol{u_l}) \boldsymbol{I} \right) \right] + \emptyset_l \mathrm{p_l} \boldsymbol{g} + \boldsymbol{F}$ | (1) |
| Continuity equation | $\frac{\partial}{\partial t} (\mathrm{p_l} \emptyset_l + \mathrm{p_g} \emptyset_g) + \nabla . (\mathrm{p_l} \emptyset_l \boldsymbol{u_l} + \mathrm{p_g} \emptyset_g \boldsymbol{u_g}) = 0$ | (2) |
| Gas-phase transport equation | $\frac{\partial \mathrm{p_g} \emptyset_g}{\partial t} + \nabla . (\mathrm{p_g} \emptyset_g \boldsymbol{u_g}) = -\boldsymbol{m_{gl}}$ | (3) |
| Gas phase velocity field | $\boldsymbol{u_g} = \boldsymbol{u_l} + \boldsymbol{u_{slip}} + \boldsymbol{u_{drift}}$ | (4) |
| Drift velocity | $\boldsymbol{u_{drift}} = -\frac{\mu_T}{\sigma_T \mathrm{p_l}} \frac{\nabla \emptyset_g}{\emptyset_g}$ | (5) |
| Bubble-induced turbulence | $\boldsymbol{S_k} = -\boldsymbol{C_k} \emptyset_g \nabla \boldsymbol{p} . \boldsymbol{u_{slip}}$ | (6) |
| Bubble-induced turbulence dissipation | $\boldsymbol{S_\varepsilon} = \frac{\varepsilon}{k} \boldsymbol{C_\varepsilon} \boldsymbol{S_k}$ | (7) |
| Turbulent dynamic viscosity (TDV) | $\mu_T = \mathrm{p} \boldsymbol{C_\mu} \frac{k^2}{\varepsilon}$ | (8) |
| Gas density from ideal gas law | $\mathrm{p_g} = \frac{(p + p_{ref}) M}{RT}$ | (9) |
| Liquid volume fraction | $\emptyset_l = 1 - \emptyset_g$ | (10) |

### 2.4 CFD Model Setup and Simulation Details

The geometrical representation of PBR systems defined in this study was symmetric. This allows for the reduction of computational domains from three-dimensional (3D) to two-dimensional (2D) versions without significantly compromising the accuracy of the computation and simulation [20, 24] (Figure 2). The 2D geometry of ALR and FPPBR in side view was simulated using a time-dependent k-ε turbulent bubbly flow model in COMSOL, considering only the liquid and gas phases. The overall numerical analysis steps were outlined based on the reported studies [13,17,20]. After the construction of geometries, all the boundary conditions required, such as the conditions for the gas inlet and gas outlet, were specified to express the behaviour of the bioreactor's operation (Table 4). Boundary 1 refers to the external surface of the gassing unit, and inlet conditions were applied where the gas and liquid conditions at this boundary are characterised by the gas flux and no-slip condition, respectively. Boundary 2, which covers gas venting and outlet conditions, was employed. For outlet conditions, the gas and liquid phases were defined as a gas outlet and a slip condition, respectively. Moreover, one point was set as a pressure constraint ($P = P_o$). Lastly, the standard wall functions and no-slip conditions were applied to the wall. The specification of boundary conditions was followed by grid generation, known as the mesh. The mesh was generated using the physics-controlled mesh setting in the software, which created unstructured triangular elements as the geometric representation of the overall 2D domains. The number of layers and the thickness adjustment factor were adjusted to increase mesh density in boundary-condition areas and around the bioreactor wall. Calculations were performed until all model parameters converged to a residual of $10^{-4,}$ and the observed parameters reached a constant value.

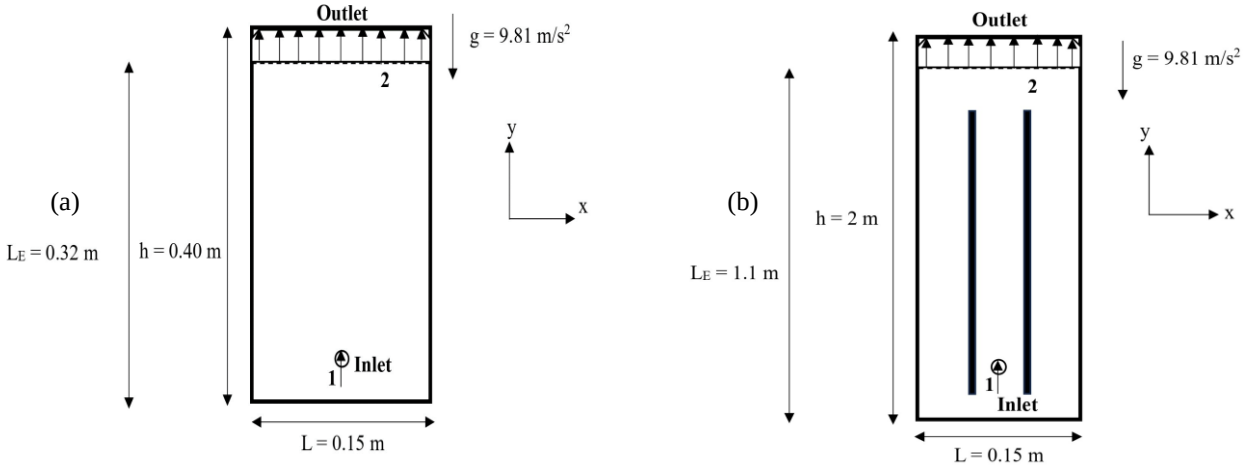


Figure 2. 2D cut of: (a) FPPBR geometry and (b) ALR geometry

Table 4. Defined boundary conditions in this analysis

| Boundary conditions | Liquid phase | Gas phase |
|---|---|---|
| Inlet | No-slip condition | Gas inlet velocity = $V_i$ m/s<br>Gas density = 0.9727 kg/m$^3$ |
| Outlet | Slip condition | Gas outlet (Degassing) |
| Wall | No gas flux at the boundary (top of reactor); non-slip model (sparger) | Velocity at the surface of the wall is zero |

### 2.5 Model Validation

The proposed CFD model in this study was validated using experimental data obtained from Sadeghizadeh et al. [26]. One of the purposes of their study was to investigate the effect of manipulating the inlet superficial gas velocity towards the flow field (liquid velocity) in the ALR system. Therefore, the CFD tool in COMSOL was used to compare the simulated liquid velocity with experimental data. This preliminary evaluation is required to verify the accuracy of the model implemented. Within the scope of this study, the methodology is developed to investigate the system's fundamental hydrodynamic characteristics. Accordingly, the findings are intended to provide foundational insights rather than a comprehensive prediction of overall reactor performance.

## 3. Results and Discussion

### 3.1 Output of Validation- ALR System Simulation

This section discusses the findings of the preliminary study's validation stage. In this part, the liquid velocity results were analysed using CFD by inputting the gas superficial velocity value based on the data specified in the study Sadeghizadeh et al. [26].

#### *3.1.1 Grid independence study*

The purpose of validation is to ensure that the model to be applied is suitable for the current application. The validation stage involved simulating the ALR system at a gas superficial velocity of 1.627 x $10^{-3}$ m/s, and grid independence studies

were conducted by varying the number of elements (grid topologies). This ensures the result obtained will be independent of the grid used. Figure 3 shows the predicted liquid velocity at different mesh element sizes obtained from the analysis. From left to right, the number of elements increased, ranging from approximately 6,000 to 90,000. The greater the number of elements, the more refined the generated grid, which requires more iterations to obtain the results. Overall, the results showed a good agreement between the experimental and numerical findings with a margin of error of less than 3%. Therefore, the implemented model is suitable for representing the problem under evaluation in this study. Aside from that, increasing the number of elements reduces error. However, as the number of elements increased to more than 20,000, the error began to deviate again, but only slightly and within an acceptable tolerance. This suggests that further grid refinement might not improve the accuracy of the results. Hence, it can be deduced that the desired error threshold was met with mesh M3, which is considered an optimal grid that provides accurate results while being computationally efficient. These grid properties will be used as the basis for the next evaluation.

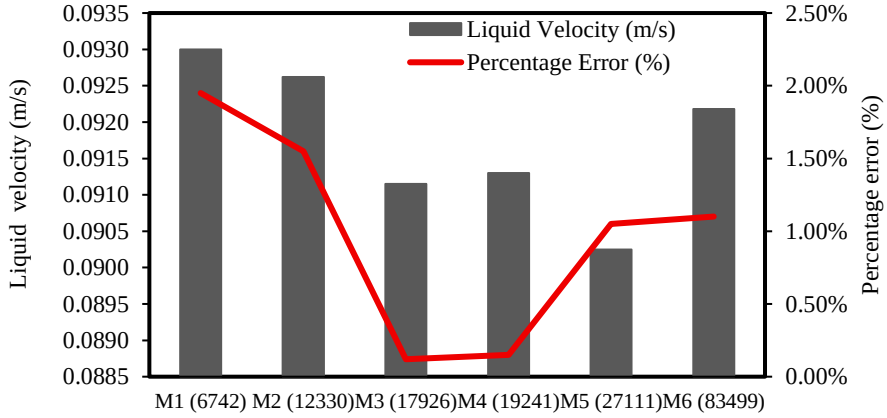


Figure 3. Simulated liquid velocity in the ALR system with variation in the number of elements

### *3.1.2 Overall COMSOL performance with respect to FPPBR simulation*

Several studies have conducted CFD analyses of FPPBR using ANSYS. This allows comparison of the current simulated results with those from past studies for validation (Table 5). Two parameters can be compared with those in previous studies: liquid velocity and TKE. The liquid velocity values were comparable to those reported by Huang et al. [27] Wang et al. [30]. However, a minor discrepancy in TKE values was observed, possibly due to the use of different models. Nevertheless, the overall fluid flow trends were similar to those identified in prior studies, corroborating the validity of the present findings. The current study and previous work [30] used the $k$–$\varepsilon$ turbulence model to represent turbulence in the FPPBR. In contrast, the past study [31] utilised the SST $k$-$\omega$ model. The current study observed a slight difference in the reported average TKE value compared to the previous work [31]. This discrepancy may be attributed to the $k$–$\varepsilon$ turbulence model's tendency to predict higher turbulence levels in the core flow region. In contrast, the SST $k$–$\Omega$ model often provides more accurate near-wall turbulence predictions [9,32]. The $k$–$\Omega$ model predicted higher TKE, indicating more vigorous turbulence and enhanced momentum transfer within the PBR, consistent with the expected increase in boundary-layer turbulence. However, the greater computational demands of the SST $k$–$\Omega$ model may present challenges for large-scale simulations [9]. Generally, the accuracy of any turbulence model depends on appropriate boundary conditions and model calibration, which are specific to the reactor configurations under study. Based on the collective results, the current model can be considered sufficiently reliable for implementation.

Table 5. Collation of current and previous findings

| Parameters | Range values | | Aeration rate (vvm) | Modelling details of previous studies | Reference |
|---|---|---|---|---|---|
| | Past | Current | | | |
| Liquid velocity (m/s) | ~0.01 | | 0 to 0.1 | Eulerian approach, Standard turbulence $k$–$\varepsilon$ model | [27,30] |
| Minimum TKE ($m^2/s^2$) | $9.767 \times 10^{-4}$ | $9.67 \times 10^{-4}$ | 0.1 | Eulerian approach, Standard turbulence $k$–$\varepsilon$ model | [30] |
| Average TKE ($m^2/s^2$) | 0.002 | 0.0017 | 0.3 | Eulerian approach, SST turbulence $k$–$\Omega$ model | [31] |

### 3.2 Analysis of Key Hydrodynamic Parameters in FPPBR

The main purpose of this study was to conduct a numerical analysis of the hydrodynamic conditions within FPPBR and to obtain a further overview of its performance. To achieve this, key hydrodynamic parameters, including overall flow structure, liquid velocity, shear stress, TDV, and TKE at different aeration rates, were further analysed and discussed.

### *3.2.1 Flow visualisation of FPPBR*

The visualisation of the flow field shows how the liquid elements circulated and moved in a specific direction within a PBR. Figure 4(a) illustrates the simulated fluid flow regime of FPPBR under 1.0 vvm aeration. An irregular fluid flow pattern was observed within the FPPBR, characterised by a dominant streamline swirl. This trend remained consistent across all aeration rates, with a slight increase in the maximum wielded velocity (Figure 4(b)). Based on the observation, the traditional design is expected to exhibit cell sedimentation at the bottom. In the conventional FPPBR design, the aeration mechanism induces mixing, and aeration is supplied solely from the bottom of the PBR via a sparger. This justifies the observed irregularity in fluid movement in the simulation. This irregularity is unfavourable because it signifies poor mixing, minimal mass transfer, and shallow light utilisation in the FPPBR system. In FPPBR, this situation is most commonly and effectively improved by installing baffles as an additional mixing tool. Several types of baffles were developed to address this issue, including double paddlewheels, inclined baffles, horizontal baffles, and waved baffles. These innovations aimed to improve operational efficiency, particularly by increasing biomass productivity [27,30,32]. This is also substantiated by the simulated flow visualisation of the ALR system, which features internal structures with a well-defined flow pattern and minimal dead zones (Figure 4 (c)).

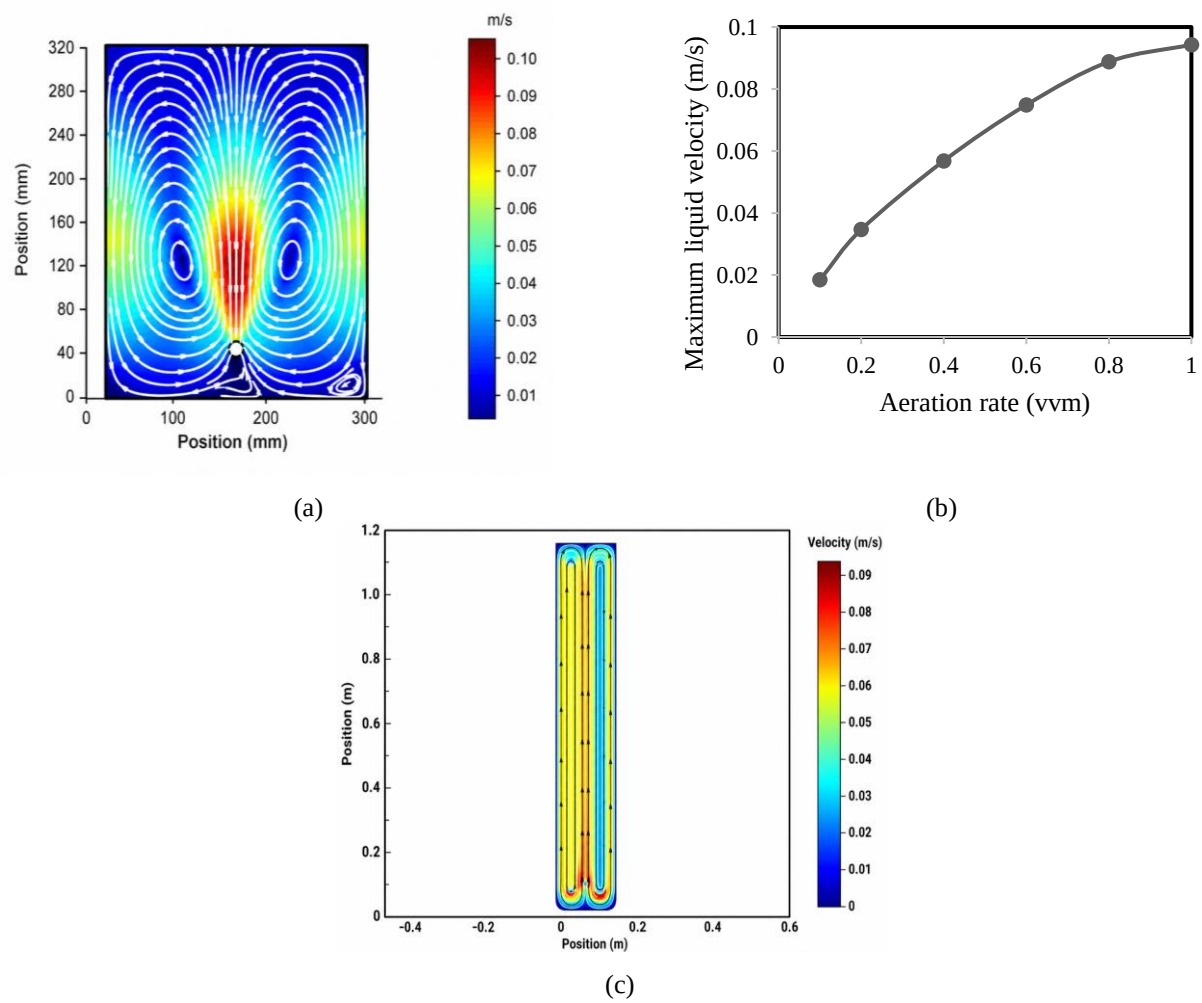


Figure 4. **(**a) Magnitude of liquid velocity (m/s) (coloured) and liquid velocity field (streamlines) in FPPBR at 1.0 vvm, (b) Maximum liquid velocity magnitude under varying aeration rates and (c) The magnitude of liquid velocity (m/s) (coloured) and liquid velocity field (streamlines) in the ALR system at an aeration rate of 0.1 vvm

When considering velocity magnitude at the same aeration rate of 0.1 vvm, it is evident that the ALR system achieved a greater liquid velocity magnitude compared to the FPPBR system. This observation justifies the crucial role of baffle installation in pneumatic PBR systems in enhancing flow structure. In addition, the maximum flow velocity in the FPPBR was observed above the gas inlet area, where fluid movement is rapid. However, the movement slowed as the distance from the inlet zone increased. The highest liquid velocity is around 9% at the gas inlet zone and exceeds 2% in other parts of the PBR, with an aeration rate of 1.0 vvm. To sum up, as the gas aeration rate rose from 0.1 to 1.0 vvm, the overall flow field profile in FPPBR improved. Nevertheless, a higher aeration rate raises concerns regarding shear stress, as it has been reported to exert greater shear stress and possibly disrupt cell development [22, 33].

### *3.2.2 Average velocity and average shear stress in FPPBR*

Figure 5 shows the effect of variation in aeration rates on average liquid velocity and average shear stress. The result shows that increasing the aeration rate increases both parameters. Generally, low- and high-velocity flows can both be

detrimental to microalgae growth. This is because high velocity causes elevated shear stress on cells, potentially disrupting cell growth. In contrast, under low-velocity conditions, algal cells accumulate and settle to the sediment. A study Wang et al. [30] considers a position within FPPBR with a velocity below 0.02 m/s as the dead zone. The average liquid velocity in the FPPBR simulation is consistently below 0.02 m/s, within the range of 0.1 to 1.0 vvm of aeration. This suggests that a significant proportion of dead zones will be present in the FPPBR, particularly near the wall, after a certain period. This issue persists and cannot be completely avoided, even with increased aeration rates. However, the extent of dead zones can be reduced at higher aeration rates, as increased velocity improves overall operational efficiency.

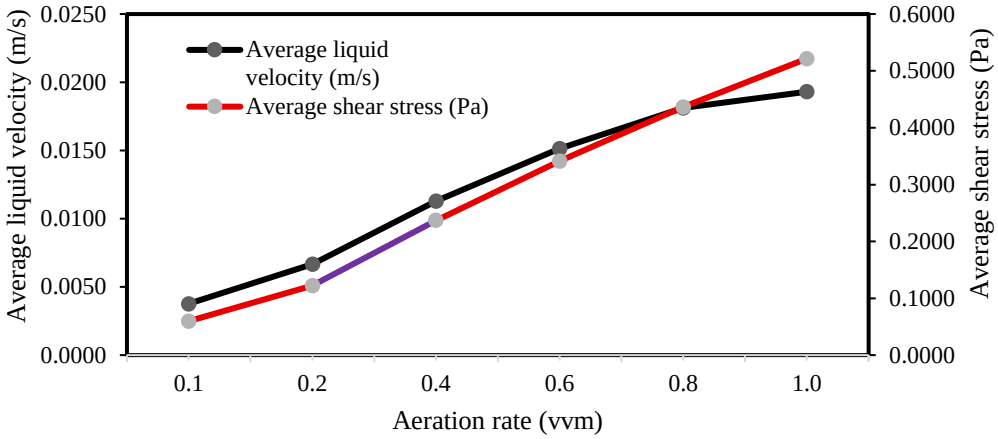


Figure 5. Average liquid velocity and average shear stress under different aeration rates

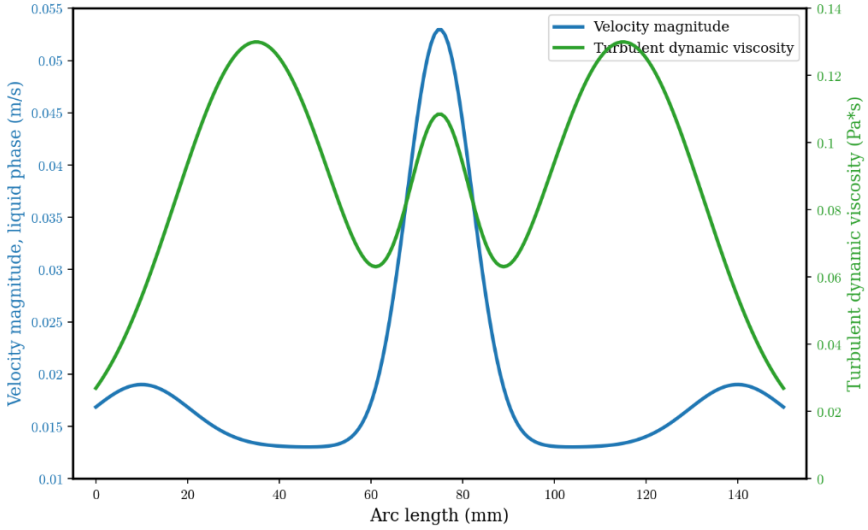


Figure 6. *x*-direction of liquid velocity (blue colour) and TDV (green colour) at 0.4 vvm

Different microalgae strains exhibit varying degrees of tolerance to shear stress. The highly sensitive strains reported are *Protoceratium reticulatum* and *Lingulodinium polyedrum*, with vital values of less than $1.6\times10^{-4}$ Pa and $4\times10^{-3}$ Pa, respectively [34]. Apart from that, Belohlav et al. [22] a critical shear stress of 0.2 Pa was identified, which could effectively inhibit or eliminate biofilm formation. Our findings reveal that an average shear stress exceeding the critical threshold of 0.2 Pa is only attained when the aeration level is maintained above 0.4 vvm. This indicates that the number of locations with shear stress below 0.2 Pa decreases when aeration exceeds 0.4 vvm. Even so, Rebej et al. [35] highlighted that aeration has a relatively minor influence on shear stress, accounting for only about 5% of the observed variations. On the contrary, the mechanical stirring process has a more pronounced effect on shear stress. TDV is an indicator of the resistance to deformation exhibited by turbulent eddies [31]. A higher TDV might indicate higher shear stress, but it will also depend on the velocity gradient [36]. This is because there is a proportional relationship between the velocity gradient and the shear rate. Referring to Figure , a notable value of TDV and velocity magnitude along the *x*-direction within FPPBR was perceived near the wall and the middle area, respectively. The middle area experienced a more pronounced shear effect than the wall area, as reflected in abrupt velocity changes over a short distance (high velocity gradient) and a slightly higher TDV. Based on the findings outlined, the aeration mechanism in the FPPBR is unlikely to cause substantial cell damage. This is because the simulated shear stress generated in the FPPBR due to aeration is lower than the most commonly declared critical value (approximately 1.2 Pa), as described by Michels et al. [37] Wang and Lan [34]. Despite this, biofilm formation or buildup can still occur when adhesion forces exceed shear forces after a certain period of continuous shear. Therefore, the best practice is to harvest biomass before it enters the death phase to ensure optimal operation and production. This determination may be achieved by evaluating growth kinetics. Considering the complex

and implicit correlation between velocity and shear stress, the recommended aeration rate to be maintained for FPPBR operation, in general, would range from 0.2 to 0.6 vvm. The suggested approach is to use a lower aeration rate in the early stages of cultivation and adjust it as cultivation progresses. However, this can affect the cultivation process in both positive and negative ways. This is because, although higher aeration is beneficial for the circulation of light and nutrients within the PBR, it can also impose a higher shear rate that could damage algal cells. Hence, further research on cultivation is still needed to assess the overall efficacy of this strategy, particularly across diverse microalgal strains.

### *3.2.3 Average TKE and average turbulent energy dissipation (TED) in FPPBR*

TKE and TED were analysed to evaluate mixing efficiency within FPPBR. Figure  depicts how the evolution of the aeration rate impacts the average TKE and average TED. The findings suggest that a higher aeration rate is associated with higher average TKE and TED values. TKE is defined as the mean kinetic energy per unit mass associated with turbulent flow eddies. Essentially, it measures the level of turbulence in a fluid flow, with a higher TKE value indicating greater fluid mixing[27,38, 39]. On the other hand, TED quantifies the energy loss due to viscous forces in turbulent flow [27]. Therefore, from the simulated result, we can observe that these parameters complement one another.

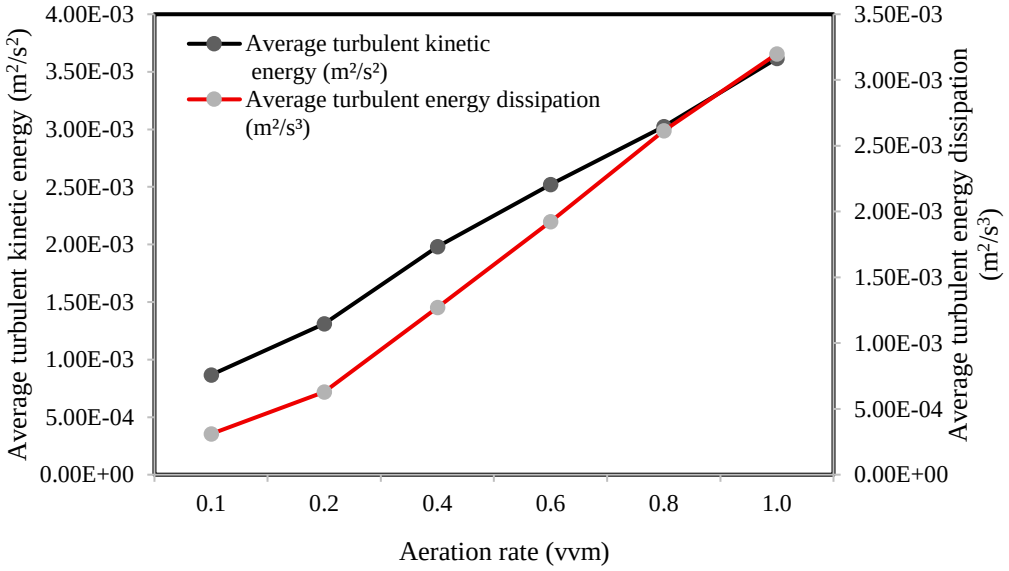


Figure 7. Effect of manipulating aeration rates on TKE and TED values

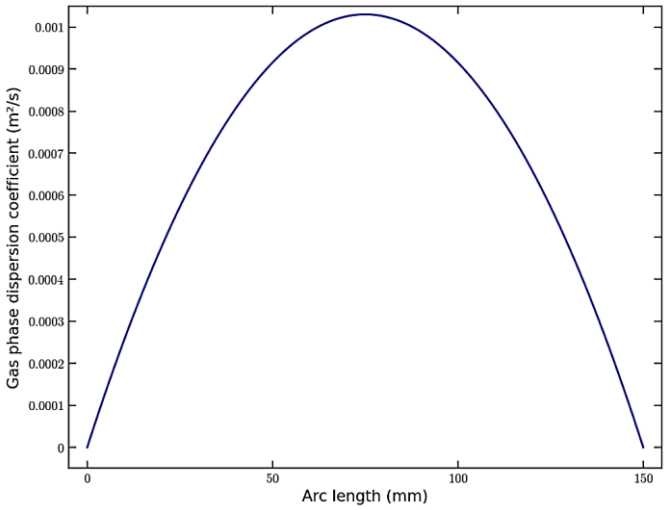


Figure 8. Gas dispersion coefficient within FPPBR across the *x*-direction with y = 80 mm at 0.4 vvm

Nevertheless, the increase of these values does not directly indicate a remarkable mixing efficiency, as a non-flat gas-phase dispersion coefficient profile was identified in the specified region within the FPPBR (Figure ). Rather, this observation strongly reflects the nonuniformity of mixing caused by turbulence. This is supported by the fact that a lower TKE was reported for the modified design FPPBR Wang et al. [30] compared to the traditional-design FPPBR. Nonetheless, the TKE field in the modified FPPBR displayed a greater homogeneity. Hence, when evaluating the TKE parameter, it is essential to focus on the uniformity of the TKE distribution rather than on the value itself. Figure 9 (a) portrays the TKE distribution within the FPPBR, revealing that the highest TKE levels were predominantly concentrated in the upper sections of the FPPBR and proximity to the sparger area. These areas are characterised by intense gas-liquid

interaction, which consequently results in greater turbulence [40]. The non-even distribution was clearly observed and could potentially be attributed to the frequency of bubble bursts [31]. Consequently, the traditional FPPBR design tends to random bubble bursts, as evidenced by the large proportion of high-TKE regions observed in this configuration. This could indicate transient light-dark zones that could potentially affect the efficiency of light utilisation for photosynthesis [40]. Moreover, Figure 9 (b) illustrates the TKE and TED values along the *x*-direction at y = 80 mm. Along the *x*-direction, the peak values of TKE and TED were detected in the middle section, while the lowest values were found at the wall, with values gradually increasing as one move away from the wall. Therefore, a turbulent effect was also present in this direction and was characterised by fluctuating patterns. Overall, although high TKE and TED may indicate high turbulent intensity, they do not guarantee mixing efficiency. As outlined by Huang et al. [27], the conventional FPPBR has higher TKE and TED values than modified designs, but the degree of mixing in the light-attenuation direction is significantly lower.

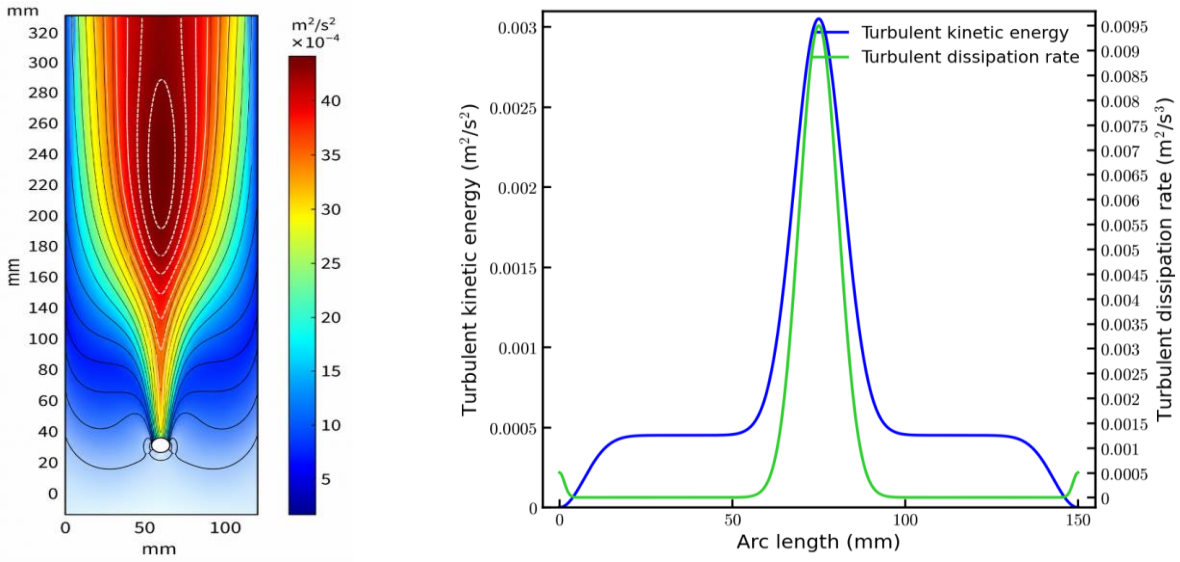


(a) (b)

Figure 9. (a) TKE profile within FPPBR at 0.4 vvm and (b) *x*-direction of TKE (blue colour) and TED (green colour) at 0.4 vvm

## 4. Conclusions

In conclusion, this study successfully achieved its objective of providing fundamental hydrodynamic insights into a conventional FPPBR using COMSOL Multiphysics®. The numerical analysis revealed that, while the traditional design exhibits satisfactory performance due to low shear stress levels that remain safely below the 1.2 Pa critical threshold for cell damage, the flow patterns remain irregular, resulting in poor mixing, limited mass transfer, and potential cell sedimentation at the bottom of the reactor. Specifically, quantitative mapping showed that average liquid velocities often fell below the 0.02 m/s dead-zone threshold and that mixing efficiency was hindered by non-uniform turbulence distribution. These novel findings highlight critical shear-sensitive regions and emphasise that, although aeration alone is insufficient for optimal mixing, adding baffles could significantly improve the flow structure. Ultimately, this study advances the CFD-based understanding of reactor hydrodynamics and provides a robust quantitative basis for future PBR design optimisation and scale-up.

**Acknowledgements**

The authors would like to express their gratitude to the International Islamic University Malaysia (IIUM), Petronas Research Sdn. Bhd. (PRSB), and Universiti Teknologi Malaysia (UTM) for providing the facilities and institutional support necessary to conduct this research.

**Funding**

Financial support from Petronas Research Sdn. Bhd. (PRSB) (Project No. SPP22-122-0122) is gratefully acknowledged.

**Declaration of Competing Interest**

The authors declare that they have no known competing financial interests or personal relationships that could have influenced the work reported in this paper.

**CRediT Authorship Contribution Statement**

Nur Aqila Syafiqa Abdul Nuri: Conceptualisation, methodology, investigation, data curation, visualisation, writing – original draft

Noor Illi Mohamad Puad: Conceptualisation, supervision, writing – review & editing

Azlin Suhaida Azmi: Funding acquisition, supervision, project administration, writing – review & editing
Farah Ahmad: Supervision, writing – review & editing
Mohd. Firdaus Abd. Wahab: Supervision, writing – review & editing
Hasrizal Abd Rahman: Project administration, writing – review & editing
Ahmad Afiq Arshad Nasharuddin: Conceptualisation, data curation

**Availability of Data and Materials**
Data sharing is not applicable to this article as no new datasets were generated or analysed in this study.

**Ethics Statement**
This study did not involve human participants or animal subjects. Ethical approval was therefore not required for this research.

**Generative Artificial Intelligence Declarations**
The authors claim that artificially intelligent-assisted technologies, such as generative AI, were not used to generate content, ideas, or theories. We have just utilised AI to enhance readability and refine the language. This was used with extreme human control and oversight. The authors take full responsibility for reviewing and approving the content.

**References**
[1] Tan XB, Lam MK, Uemura Y, Lim JW, Wong CY, Lee KT. Cultivation of microalgae for biodiesel production: A review on upstream and downstream processing. Chinese Journal of Chemical Engineering. 2018;26(1):17–30. https://doi.org/10.1016/j.cjche.2017.08.010
[2] Vale MA, Ferreira A, Pires JCM, Gonçalves AL. $CO_2$ capture using microalgae. In: Advances in carbon capture. Woodhead Publishing; 2020. p. 381–405. https://doi.org/10.1016/B978-0-12-819657-1.00017-7
[3] Alok A, Shrestha R, Ban S, Devkota S, Uprety B, Joshi R. Technological advances in the transformative utilisation of CO2 to value-added products. Journal of Environmental Chemical Engineering. 2022;10(1):106922.https://doi.org/10.1016/j.jece.2021.106922
[4] Barbosa MJ, Janssen M, Südfeld C, D'Adamo S, Wijffels RH. Hypes, hopes, and the way forward for microalgal biotechnology. Trends in Biotechnology. 2023; 41(3):452–71. DOI: 10.1016/j.tibtech.2022.12.017
[5] Huang Q, Jiang F, Wang L, Yang C. Design of photobioreactors for mass cultivation of photosynthetic organisms. Engineering. 2017;3(3):318–29. https://doi.org/10.1016/J.ENG.2017.03.020
[6] Zhou W, Lu Q, Han P, Li J. Microalgae cultivation and photobioreactor design. In: Microalgae cultivation for biofuels production. Academic Press; 2020. p. 31–50. https://doi.org/10.1016/B978-0-12-817536-1.00003-5
[7] Benner P, Meier L, Pfeffer A, Krüger K, Oropeza Vargas JE, Weuster-Botz D. Lab-scale photobioreactor systems: principles, applications, and scalability. Bioprocess and Biosystems Engineering. 2022;45(5):791–813. https://doi.org/10.1007/s00449-022-02711-1
[8] Chu HM, Narindri B, Hsueh HT, Chu H. Improvement of *Thermosynechococcus* sp. CL-1 performance on biomass productivity and $CO_2$ fixation via growth factors arrangement. Journal of Photochemistry and Photobiology B: Biology. 2020;205:111822. https://doi.org/10.1016/j.jphotobiol.2020.111822
[9] Luzi G, McHardy C. Modeling and simulation of photobioreactors with computational fluid dynamics—A comprehensive review. Energies. 2022;15(11):3966. https://doi.org/10.3390/en15113966
[10] Pires JCM, Alvim-Ferraz MCM, Martins FG. Photobioreactor design for microalgae production through computational fluid dynamics: A review. Renewable and Sustainable Energy Reviews. 2017;79:248–54. https://doi.org/10.1016/j.rser.2017.05.064
[11] Ranganathan P, Pandey AK, Sirohi R, Tuan Hoang A, Kim SH. Recent advances in computational fluid dynamics (CFD) modelling of photobioreactors: Design and applications. Bioresource Technology. 2022;350:126920. https://doi.org/10.1016/j.biortech.2022.126920
[12] Ansoni JL, Santiago PA, Seleghim Jr. P. Multiobjective optimisation of a flat-panel airlift reactor designed by computational fluid dynamics. Chemical Engineering Science. 2019;195:946–57. https://doi.org/10.1016/j.ces.2018.10.041
[13] Ali H, Solsvik J, Wagner JL, Zhang D, Hellgardt K, Park CW. CFD and kinetic-based modeling to optimize the sparger design of a large-scale photobioreactor for scaling up of biofuel production. Biotechnology and Bioengineering. 2019;116(9):2200–11. https://doi.org/10.1002/bit.27010
[14] Vasile NS, Cordara A, Usai G, Re A. Computational Analysis of dynamic light exposure of unicellular algal cells in a flat-panel photobioreactor to support light-induced $CO_2$ bioprocess development. Frontiers in Microbiology. 2021;12: 639482.https://doi.org/10.3389/fmicb.2021.639482
[15] Assunção J, Malcata FX. Enclosed "non-conventional" photobioreactors for microalga production: A review. Algal Research. 2020;52:102107. https://doi.org/10.1016/j.algal.2020.102107
[16] Peter AP, Koyande AK, Chew KW, Ho SH, Chen WH, Chang JS, Krishnamoorthy R, Banat F, Show PL. Continuous cultivation of microalgae in photobioreactors as a source of renewable energy: current status and future challenges. Renewable and Sustainable Energy Reviews. 2022;154:111852. https://doi.org/10.1016/j.rser.2021.111852
[17] Li M, Hu D, Liu H. Photobioreactor with ideal light–dark cycle designed and built from mathematical modeling and CFD simulation. Ecological Engineering. 2014;73:162–7. https://doi.org/10.1016/j.ecoleng.2014.09.010

[18] Gómez-Pérez CA, Espinosa J, Montenegro Ruiz LC, van Boxtel AJB. CFD simulation for reduced energy costs in tubular photobioreactors using wall turbulence promoters. Algal Research. 2015;12:1–9. https://doi.org/10.1016/j.algal.2015.07.011
[19] Gómez-Pérez CA, Espinosa Oviedo JJ, Montenegro Ruiz LC, van Boxtel AJB. Twisted tubular photobioreactor fluid dynamics evaluation for energy consumption minimisation. Algal Research. 2017;27:65–72. https://doi.org/10.1016/j.algal.2017.08.019
[20] Hinterholz CL, Trigueros DE, Módenes AN, Borba CE, Scheufele FB, Schuelter AR, Kroumov AD. Computational fluid dynamics applied for the improvement of a flat-plate photobioreactor towards high-density microalgae cultures. Biochemical Engineering Journal. 2019;151:107257. https://doi.org/10.1016/j.bej.2019.107257
[21] Inostroza C, Solimeno A, García J, Fernández-Sevilla JM, Acién FG. Improvement of real-scale raceway bioreactors for microalgae production using computational fluid dynamics (CFD). Algal Research. 2021;54:102207. https://doi.org/10.1016/j.algal.2021.102207
[22] Belohlav V, Zakova T, Jirout T, Kratky L. Effect of hydrodynamics on the formation and removal of microalgal biofilm in photobioreactors. Biosystems Engineering. 2020;200:315–27. https://doi.org/10.1016/j.biosystemseng.2020.10.014
[23] Huang J, Kang S, Wan M, Li Y, Qu X, Feng F, Wang J, Wang W, Shen G, Li W. Numerical and experimental study on the performance of flat-plate photobioreactors with different inner structures for microalgae cultivation. Journal of Applied Psychology. 2015;27:49–58. https://doi.org/10.1007/s10811-014-0281-y
[24] Yaqoubnejad P, Rad HA, Taghavijeloudar M. Development a novel hexagonal airlift flat plate photobioreactor for the improvement of microalgae growth that simultaneously enhance $CO_2$ bio-fixation and wastewater treatment. Journal of Environmental Management. 2021;298:113482. https://doi.org/10.1016/j.jenvman.2021.113482
[25] Zhang X. Microalgae removal of CO2 from flue gas. IEA Clean Coal Cent UK. 2015.
[26] Sadeghizadeh A, Farhad Dad F, Moghaddasi L, Rahimi R. $CO_2$ capture from air by *Chlorella vulgaris* microalgae in an airlift photobioreactor. Bioresource Technology. 2017;243:441–7. https://doi.org/10.1016/j.biortech.2017.06.147
[27] Huang J, Li Y, Wan M, Yan Y, Feng F, Qu X, et al. Novel flat-plate photobioreactors for microalgae cultivation with special mixers to promote mixing along the light gradient. Bioresource Technology. 2014;159:8–16. https://doi.org/10.1016/j.biortech.2014.01.134
[28] Salehpour R, Jalilnejad E, Nalband M, Ghasemzadeh K. Hydrodynamic behaviour of an airlift reactor with net draft tube with different configurations: Numerical evaluation using CFD technique. Particuology. 2020;51:91–108. https://doi.org/10.1016/j.partic.2019.09.005
[29] COMSOL Inc. COMSOL Multiphysics® v. 6.0 Documentation [Internet]. COMSOL AB; 2021. Retrieved from: https://doc.comsol.com/6.0/docserver/#!/com.comsol.help.comsol/helpdesk/helpdesk.html
[30] Wang L, Wang Q, Zhao R, Tao Y, Ying KZ, Mao XZ. Novel flat-plate photobioreactor with inclined baffles and internal structure optimisation to improve light regime performance. ACS Sustainable Chemistry & Engineering. 2021;9(4):1550–8. https://doi.org/10.1021/acssuschemeng.0c06109
[31] Guler BA, Deniz I, Demirel Z, Oncel SS, Imamoglu E. Comparison of different photobioreactor configurations and empirical computational fluid dynamics simulation for fucoxanthin production. Algal Research. 2019;37:195–204. https://doi.org/10.1016/j.algal.2018.11.019
[32] Besagni G, Inzoli F, Ziegenhein T. Two-Phase Bubble Columns: A Comprehensive Review. ChemEngineering. 2018;2(2):13. https://doi.org/10.3390/chemengineering2020013
[33] Xu J, Cheng J, Lai X, Zhang X, Yang W, Park JY, et al. Enhancing microalgal biomass productivity with an optimised flow field generated by double paddlewheels in a flat plate photoreactor with $CO_2$ aeration based on numerical simulation. Bioresource Technology. 2020;314:123762. https://doi.org/10.1016/j.biortech.2020.123762
[34] Pawar SB. Computational fluid dynamics (CFD) analysis of airlift bioreactor: effect of draft tube configurations on hydrodynamics, cell suspension, and shear rate. Bioprocess and Biosystems Engineering. 2018;41(1):31–45. https://doi.org/10.1007/s00449-017-1841-8
[35] Wang C, Lan CQ. Effects of shear stress on microalgae – A review. Biotechnology Advances. 2018;36(4):986–1002. https://doi.org/10.1016/j.biotechadv.2018.03.001
[36] Rebej M, Juřena T, Vondál J, Fuente Herraiz D, Červený J, Jegla Z. Numerical simulations and validation of single- and two-phase flow in a stirred lab-scale photobioreactor. Biosystems Engineering. 2023;230:35–50. https://doi.org/10.1016/j.biosystemseng.2023.04.004
[37] Belohlav V, Uggetti E, García J, Jirout T, Kratky L, Díez-Montero R. Assessment of hydrodynamics based on computational fluid dynamics to optimise the operation of hybrid tubular photobioreactors. Journal of Environmental Chemical Engineering. 2021;9(5):105768. https://doi.org/10.1016/j.jece.2021.105768
[38] Michels MHA, van der Goot AJ, Norsker NH, Wijffels RH. Effects of shear stress on the microalgae *Chaetoceros muelleri*. Bioprocess and Biosystems Engineering. 2010;33(8):921–7. https://doi.org/10.1007/s00449-010-0415-9
[39] Li L, Xu X, Wang W, Lau R, Wang CH. Hydrodynamics and mass transfer of concentric-tube internal loop airlift reactors: A review. Bioresource Technology. 2022;359:127451. https://doi.org/10.1016/j.biortech.2022.127451
[40] Luo HP, Al-Dahhan MH. Local characteristics of hydrodynamics in draft tube airlift bioreactor. Chemical Engineering Science. 2008; 63(11):3057–68. https://doi.org/10.1016/j.ces.2008.03.015